Spin-isospin flip giant resonances and shell dependence in ^{7}Li and ^{9}Be by π^+ photoproduction

K. Shoda, S. Tôyama,* K. Takeshita,† and T. Kobayashi‡
Laboratory of Nuclear Science, Tohoku University, Sendai 989-0826, Japan

H. Tsubota
Department of Physics, Graduate School of Science, Tohoku University, Sendai 980-8578, Japan
(Received 1 December 1997)

The giant resonances of spin-isospin flip mode are studied by measuring the energy and angular distributions of π^+ electroproduced from ^{7}Li and ^{9}Be nuclei. Several strong π^+ groups are found and angular distributions of these groups are analyzed by distorted-wave impulse approximation calculations using the single particle shell model. The experimental cross section of the groups corresponds to an order of the charge exchange single particle transition strength, establishing them as spin-isospin flip giant resonances. The shell model nature of (γ,π^+) results for $1p_{3/2}$ shell nuclei are summarized and presented together with previously published data. The obtained results are compared to previously published data for (π^-,γ), (n,p), $(e,e'p)$, and $(p,2p)$ reactions. Strong transitions consistent with the giant resonance excitations from the $1s_{1/2}$ shell in the core and from the $1p_{3/2}$ valence shell are observed. [S0556-2813(99)03106-4]

PACS number(s): 25.20.Lj, 21.10.Jx, 24.30.Cz, 27.20.+n

I. INTRODUCTION

The single particle shell model and the cluster model have been applied to the examination of the properties of nuclear states and reactions. These models are used in different modes to find an approximation to the solution of the many-nucleon Schrödinger equation, which cannot be solved rigorously.

The $1p_{3/2}$ shell nuclei are often proven to be explained by a cluster model based on the α-cluster and other clusters formed by some of the $1s_{1/2}$ shell nucleons. For example, the light nuclei with masses $A=4-8$ have been very well described mostly by the two body cluster model theory. Nuclei having masses $A>8$ become tedious to treat using the cluster theory, because more than three clusters are concerned. Application of the complete cluster model appears to be insufficient in the $A>8$ nuclei, even in ^{12}C and ^{16}O, which sometimes show cluster construction clearly. The recent development of the cluster model is summarized by Langanke [1].

The nuclei ^{6}Li and ^{7}Li are described by the cluster model quite well using the most important component of $[\alpha\cdot d]$, $[^3\mathrm{He}\cdot t]$ and $[\alpha\cdot t]$. These configurations have also been studied using the microscopic cluster model. For ^{9}Be, the cluster model has been partially studied using the cluster components of $[\alpha\cdot\alpha\cdot n]$ and $[^5\mathrm{He}\cdot\alpha]$. A good qualitative explanation is obtained for the photodisintegrations of this nucleus, as in the case of ^{6}Li and ^{7}Li [2].

The shell model nature seems to be obscure in ^{6}Li, ^{7}Li, and ^{9}Be. The shell model of these nuclei have been examined with respect to the Q value of the single particle in the shell via $(e,e'p)$ and $(p,2p)$ experiments and with respect to the giant resonance measured by the (n,p) reaction. These results will be discussed in comparison with those of the (γ,π^+) reaction.

In the present paper, the single particle shell model nature is investigated by examining the character of the single nucleon interaction in the (γ,π^+) reaction for the giant resonance in $1p_{3/2}$ shell nuclei, which indicate cluster nature. The states that can be examined using the (γ,π^+) reaction are limited by the selection rule for spin-isospin flip mode of the single particle transition in this reaction. Therefore, the present study enables to select the states to be examined than is the case for the $(e,e'p)$, $(p,2p)$ and (n,p) reactions, which include several overlapping states leading to a broad resonance shape. Such selectivity in the (γ,π^+) reaction for shell model nature should provide greater clarity, even in nuclei which are well described by the cluster model.

The cross sections of the pion photoproduction from nuclei are given in impulse approximation [3] as

$$\left(\frac{d\sigma}{d\Omega}\right)_{(\gamma,\pi)}=\frac{p}{km_\pi^2}e^2f^2\frac{1}{2J_i+1}\times\sum_{M_iM_f}\sum_{\lambda}|\langle J_fM_f|\phi_\pi^*F|J_iM_i\rangle|^2, \quad (1)$$

where $e^2=1/137$, $f^2=0.08$, k and p are the momenta of the incident photon and outgoing pion, respectively, m_π is the pion rest mass, λ is the photon polarization, ϕ_π is the pion wave function, and $|J_iM_i\rangle$ and $|J_fM_f\rangle$ are the initial and final nuclear states, respectively. The operator F is given in terms of elementary $\pi^\pm$ photoproduction operator F_n as

$$F=\sum_{n=1}^{A}F_n, \quad (2)$$

*Present address: Tokai Works, Power Reactor and Nuclear Fuel Development Corporation, Tokaimura, Ibaraki 311-1393, Japan.
†Present address: Spring-8 ring A, Japan Synchrotron Radiation Research Institute, Hyogo 678-12, Japan.
‡Present address: College of Radiology, Teikyo University, Hachioji, Tokyo 173-8605, Japan.

$$F_n = \vec{J}_5 \cdot \vec{\varepsilon}_\lambda \exp(i\vec{k}\cdot\vec{r}_n)\tau^{\pm}, \quad (3)$$

where $\vec{J}_5$ is a pseudovector operator, $\vec{\varepsilon}_\lambda$ and $\vec{k}$ are the vector of polarization and momentum of photon, respectively, and $\tau^{\pm}$ is the isospin raising or lowering operator. The operator F_n is given by various expressions and consists of two terms, the Born term describing the nonresonance excitation and the resonance term describing the Δ excitation. Based on the theoretical analysis and fitting to the experimental cross section, the Born term corresponds to the continuous cross section and the resonance term is strong in the Δ-resonance region at around 330 MeV. In the threshold region less than 200 MeV, the main operator is the Born term and the effect of the Δ resonance is very small [3].

The interaction operators in the Born term are composed of the main parts, including the intrinsic nucleon spin operator $\vec{\sigma}$ leading to the spin flip component and an additional small part of the spin nonflip component. The Born term at around the threshold energy is expressed by the Kroll-Ruderman term $\vec{\sigma}\cdot\vec{\varepsilon}_\lambda\tau^{\pm}$. In the energy region from the threshold to about 200 MeV, the nuclear transition in the charged pion photoproduction can be approximated by the spin-isospin flip transition. When ϕ_π is given by the partial wave expansion, the matrix elements in Eq. (1) can be expressed by the multipole transition densities for momentum transfer $\vec{q}=\vec{k}-\vec{p}$. Therefore, the reaction depends on the momentum transfer fixed by the photon momentum and the pion momentum on the ejection angle. In the present paper, the entire term of the interaction operator is used to analyze the experimental results.

Similar studies have initially been made by radiative capture of stopped π^- by nucleus [(π^-,γ) reaction], which is described similar to Eqs. (1)–(3), as a reaction inverse of (γ,π^+) process under the limited condition that k is less than the threshold value, $p\approx 0$ and the pion wave function ϕ_π corresponds to the $1s$ and $2p$ pion orbital momentum in the pionic atom. Here, momentum transfer of radiative pion capture is fixed without angular dependence and is approximately equal to that of the (γ,π^+) reaction for a π^+ ejection angle of around 30° and a photon energy about 200 MeV.

The results of the present study revealed that the momentum transfer can vary in the (γ,π^+) reaction by changing the detection angle, whereas in the (π^-,γ) reaction, the momentum transfer is fixed using stopped π^-. The possible variation in momentum transfer enables the nuclear information to be examined by measuring the π^+ angular distribution in order to find various multipole spin-isospin flip transitions. This is in contrast to the (π^-,γ) reaction showing the lowest multipole spin-isospin flip transition. The results of the (π^-,γ) reaction are compared to the present (γ,π^+) results later in the present paper.

Unlike the nucleon, the photon can penetrate into the nuclear interior when used to initiate a reaction. The impulse approximation for an individual nucleon is much better in the (γ,π^+) and (π^-,γ) reactions when a short wavelength photon of 100–200 MeV is used than in the photonuclear reaction when a long wavelength photon of approximately 20 MeV is used. The cluster nature of the nuclei can be studied using the photonuclear reaction and the long wavelength photon, which is better matched to the cluster motion during the nuclear collective motion around the nuclear giant resonance. The charged photopion production study using the short wavelength photon give good information on nuclear shell model nature, even when the nuclei are well described by the cluster model. The pion produced by the (γ,π^+) reaction interacts with the nucleons inside the nucleus. This effect can be estimated using the optical potential deduced from pion scattering on the nuclei.

The present experiment examines the spin-isospin flip mode in the $1p_{3/2}$ shell nuclei using the single particle shell model by impulse approximation. Previous (γ,π^+) data show the spin-isospin flip giant resonance leading to the

TABLE I. Parameters of the experiment.

Target (natural metal)	^{7}Li	^{9}Be
Target thickness (mg/cm^2)	121–200[a]	129
Electron energy (MeV)	203	204
π^+ detection angle (degrees) 30, 60, 90, 120, 150		
Measured π^+ energy (MeV)	20–50	22–52
π^+ energy uncertainty[b] (MeV)	±0.6	±0.5

[a]The thickness was changed depending on the detection angle.
[b]Average estimation at π^+ energy around 30 MeV, which corresponds to approximately 20 MeV for the residual states.

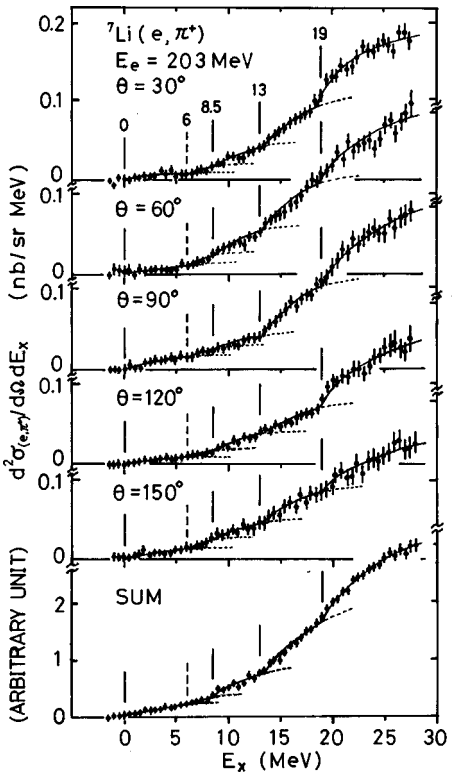

FIG. 1. Energy distribution of π^+ electroproduced from ^{7}Li at five angles as a function of E_x given by $E_x = E_0 - E_{\text{threshold}} - T_\pi$. Here, E_0 is 203 MeV. The sum spectrum (at bottom) is given by summation over all angles in order to improve statistics. Vertical lines show E_{x_i} the central energy of the resonance at the residual state for strong photopion transition determined by the χ^2 fit with the sum spectrum. The solid curves indicate the results by sum of the spectra for the individual resonances determined by the χ^2 fit with Eqs. (5)–(8).

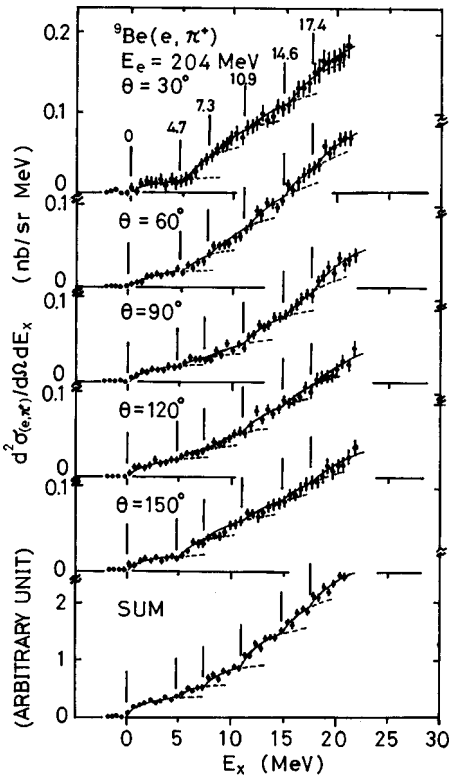

FIG. 2. Energy distribution of π^+ electroproduced from ^{9}Be (see caption for Fig. 1). Here, E_0 is 204 MeV.

ground and low lying states and, in some cases, up to high lying residual states for the target nuclei, ^{6}Li [4], ^{9}Be [5], ^{12}C [6–8], and ^{13}C [8–10]. In the present study, the spin-isospin flip giant resonances leading to highly excited residual states on ^{7}Li and ^{9}Be are studied in order to discuss $1\hbar\omega$ transitions in $1p_{3/2}$ shell nuclei.

II. EXPERIMENTAL PROCEDURES AND RESULTS

Experiments were conducted using the 300 MeV electron linear accelerator at Tohoku University. Electron beams having kinetic energies of 203 and 204 MeV and resolutions of ± 0.5 MeV irradiated the Li and Be targets, respectively, and the produced π^+ were momentum analyzed by a 169.7° double-focusing magnetic spectrometer. For the ^{7}Li experiment, the detector system consisted of a 33-channel triple coincidence detector array set along the focal plane [6]. For the ^{9}Be experiment, three layers of MWPC were used, set along the focal plane, followed by a backup counter for particle identification [11]. The main parameters of the experiment are listed in Table I.

The results for ^{7}Li and ^{9}Be are plotted in Figs. 1 and 2, in which the abscissas are transformed from pion energy T_π to $E_x = E_0 - E_{\text{threshold}} - T_\pi$ corrected for kinematics, where E_0 is the electron kinetic energy. This is convenient for later analysis. For each target, the figure shows the spectra at the five pion angles, 30°, 60°, 90°, 120° and 150°. The sum spectra for all of the angles were obtained for improved statistics and in order to determine the most probable resonance energies and is shown at the bottom of each figure. The results show some breaks as indicated by vertical lines.

The measured energy distributions of π^+ are the sum of the result electroproduced and that photoproduced by bremsstrahlung produced in the target. The bremsstrahlung spectra corresponding to the present experimental parameters were calculated using the formula given by Schiff [12]. Electroproduction can be described as photoproduction by virtual photons associated with electrons. The virtual photon spectra are calculated using the formula by Tiator and Wright [13] for pion production. The photon spectra $N(E_\gamma)$ are then the summation of the spectra of the virtual photons and the bremsstrahlung. The latter accounts for less than 10% of the total photons in the present experiment. The photon spectra $N(E_\gamma)$ are continuous, showing a sudden increase at the endpoint energy E_0 (the maximum E_γ) that is equal to the electron kinetic energy. The absolute value of $N(E_\gamma)$ was confirmed by comparing the measured π^+ spectrum of hydrogen in the LiH target using the known hydrogen cross section.

The energy spectra of π^+ produced by the photon given by $N(E_\gamma)$ can be expressed as a function of the pion energy as

$$\frac{d^2\sigma_{(e,\pi)}(T_\pi)}{d\Omega dT_\pi} = \int_0^{E_0} \frac{d\sigma_{(\gamma,\pi)}(E_\gamma, E_x)}{d\Omega} N(E_\gamma) dE_\gamma. \quad (4)$$

Here, the cross section $\sigma_{(\gamma,\pi)}(E_\gamma, E_x)$ is a function of photon energy E_γ and residual energy E_x. As a function of E_γ the cross sections expected to change gradually to zero at the threshold; however, as a function of E_x corresponding to the nuclear structure of the residual nucleus, the cross section should indicate some resonances and continuums. The purpose here is to investigate the E_x dependence of the (γ, π^+) cross section.

Based on the result of the π^+ energy distribution in the (γ, π^+) reaction measured using tagged photon on ^{12}C and ^{13}C, the cross sections as a function of E_x indicate well separated groups having FWHMs of about 2 MeV composing a broad resonance shape centered at about 7 MeV and a FWHM of about 12 MeV on a small continuum cross section [8]. Since the energy resolution of the pion detectors in this experiment is about 2 MeV, each group corresponds to a single or complex narrow residual state. The π^+ spectra in the present (e, π^+) reaction are given by folding of the continuous photon spectrum $N(E_\gamma)$ on the (γ, π^+) cross section as given by Eq. (4). Since $N(E_\gamma)$ shows a sudden increase at the endpoint energy E_0 of E_γ, the breaks in the π^+ spectra reflect the structure of the (γ, π^+) cross section.

The π^+ spectra of the test samples are calculated by folding of the photon spectrum on some typical test cross sections. These test cross sections are taken as a continuum, resonances described by the Lorentz shape at a central energy E_{x_i} having FWHMs of 4 and 2 MeV and the line shape. The two resonances and the line shape are normalized to the same integrated cross section and are assumed to be constant in the region about 25 MeV lower than E_0. For the continuum cross section, the integrated cross section within 20 MeV in the endpoint energy region is normalized to the value for the resonances. The results are shown in Fig. 3.

Figure 3 shows that the continuum cross section of the (γ, π^+) reaction leads to a gradually changing continuum π^+ spectrum. In the case of Lorentz shape (γ, π^+) cross section, the π^+ spectra can be approximated using a refer-

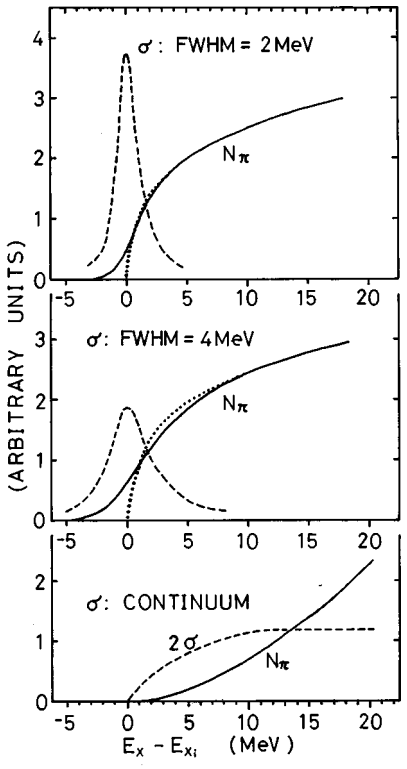

FIG. 3. Test examples of π^+ spectra calculated by folding of photon spectrum $N(E_\gamma)$ on (γ,π^+) cross sections of two Lorentz shape resonances having FWHMs of 2 and 4 MeV and a line shape cross section. The π^+ spectrum by folding on a continuum (γ,π^+) cross section is also shown. The results are normalized to the same integrated (γ,π^+) cross sections. The curves show the (γ,π^+) cross sections (broken lines), π^+ spectra (solid lines) and the π^+ spectrum with line shape cross section (reference spectrum; dotted lines).

ence spectrum given by the line shape resonance. The reference spectrum is equivalent to the pattern of the photon spectrum $N(E_\gamma)$ that shows a sudden increase at the endpoint energy. Only the spectra around the endpoint are sensitive to the resonance width. Estimation of the width may be possible using the shape of the spectra in this region. However, using the method to determine the width from the results shown in Figs. 1 and 2 is difficult because the statistics of the spectrum alone are not sufficient to define the shape in the corresponding region.

When the π^+ spectra can be approximately fitted using the pattern of the photon spectrum, both the central energy and the integrated cross section of the resonances are estimated using the reference spectrum, as shown in Fig. 3. The figure shows that this approximation analysis appears to be good when the FWHM of the Lorentz shape is smaller than 2 MeV, which is nearly equal to the tagged photon results including the detector resolution on ^{12}C and ^{13}C. For FWHMs$\approx$2 and 4 MeV in the Lorentz shape, the uncertainty of the central energy of the resonance determined by this fitting may be about 0.5 and 1 MeV, respectively. Other similar test calculations using Gauss type resonance of FWHM$\approx$4 MeV have also been made, and these calculations indicate that the result is similar to that for the Lorentz shape of FWHM$\approx$2 MeV rather than 4 MeV, thus a much better approximated result is given if the resonance is the Gauss type.

The spectra for the Lorentz shape resonances in Fig. 3 agree well with the reference spectrum in the region far greater than about 1.5 times the energy of the FWHM from the central energy. Therefore, a good estimation of the integrated cross section of the resonance will be obtained by fitting the reference spectrum in this energy region.

In the analysis of the π^+ spectra for the purpose of investigating the central energy and integrated cross section of the resonances, approximation is generally performed by fitting in the region around 5 MeV, far from the break points with the reference spectrum, which is equivalent to the pattern of the photon spectrum $N(E_\gamma)$.

When the line shape is applied for the resonances in the (γ,π^+) cross section, Eq. (4) is expressed as

$$\frac{d^2\sigma_{(e,\pi)}(T_\pi)}{d\Omega dT_\pi}=\sum_i\left(\frac{d\sigma_{(\gamma,\pi)}(E_{x_i})}{d\Omega}\right)_i\left[N(E_\gamma)\frac{dE_\gamma}{dT_\pi}\right]_i+C(T_\pi), \tag{5}$$

$$E_\gamma=E_{\text{threshold}}+E_{x_i}+T_\pi, \tag{6}$$

where subscript i indicates the individual residual states and $C(T_\pi)$ is the continuum part of the pion spectra. The sudden increase at energy $T_\pi(i)$ corresponds to the individual residual energy E_{x_i} as given by

$$E_0=E_{\text{threshold}}+E_{x_i}+T_\pi(i). \tag{7}$$

The π^+ spectra in Figs. 1 and 2 are plotted as $(d^2\sigma_{(e,\pi)}/d\Omega dE_x)$ using a function of E_x, where

$$E_x=E_0-E_{\text{threshold}}-T_\pi. \tag{8}$$

Here, when sudden increases appear in the spectra at $E_x=E_{x_i}$, Eq. (8) is equivalent to Eq. (7) for the maximum energy $T_\pi(i)$. Therefore, the spectra indicate the strong transitions leaving the residual states at E_{x_i}.

The curves in Figs. 1 and 2 show the results determined by a χ^2 fit with Eqs. (5)–(8) using the reference spectrum at E_{x_i}, which is determined from the sum spectra of all of the angles. The figures show the spectra by fitting at individual E_{x_i} and the sum of the individual spectra. By this fitting, the most probable values of the differential photopion cross sections $(d\sigma_{(\gamma,\pi)}/d\Omega)_i$ are determined. The cross section is approximated as constant in the photon energy region of several MeV at around the end point energy E_0. In the present method, the average photon energy E_γ for the obtained cross section is slightly less than E_0, because the photon spectrum is zero at E_0 and moves toward lower energy in the fitting energy region. The most probable photon energy having sufficient photon number in the χ^2 fit for the cross section is estimated as $E_\gamma=E_0-2$ MeV; however, the results are not sensitive to E_γ within several MeV.

As shown in Figs. 1 and 2, the experimental π^+ energy distributions are well fitted to the sum of individual resonances without continuum spectrum. This shows that the contribution of the continuum (γ,π^+) cross section appears to be very small, because such a cross section corresponds to a gradually changing π^+ spectrum, as shown in Fig. 3. However, such a conclusion may not be valid because the present

TABLE II. Differential cross sections (γ,π^+) on ^{7}Li and ^{9}Be determined by a χ^2 fit. Due to large statistical error in the region below 8.5 MeV on ^{7}Li and below 4.7 MeV on ^{9}Be, only average values are shown.

E_{x_i} (MeV)		$d\sigma/d\Omega$ (μb/sr) θ (degrees)				
		30	60	90	120	150
^{7}Li	0			~0.2 (average)		
	~6			~0.3 (average)		
	8.5	0.44±0.09	0.47±0.14	0.22±0.11	0.33±0.09	0.27±0.11
	13.0	0.92±0.21	1.40±0.52	1.08±0.43	0.48±0.14	0.43±0.12
	19.0	1.53±0.40	2.00±0.40	1.73±0.30	1.15±0.25	0.55±0.12
^{9}Be	0			~0.2 (average)		
	4.7	0.69±0.24	0.33±0.11	0.11±0.07	0.14±0.08	0.32±0.08
	7.3	1.00±0.29	0.94±0.17	0.39±0.20	0.34±0.13	0.32±0.12
	10.9	0.5±0.9	0.87±0.13	0.86±0.16	0.82±0.18	0.30±0.11
	14.6	0.71±0.24	0.71±0.20	0.57±0.23	0.34±0.25	0.35±0.14
	17.4	0.6±1.0	0.73±0.26	0.83±0.25	0.54±0.17	0.41±0.34

analysis is based on the assumption that the resonances are constant in the endpoint region of photon energy extending up to about (25-E_{x_i}) MeV. If this assumption is not satisfied and the cross section decreases in smaller photon energy for example, the spectra summed for all resonances should require an additional continuum cross section to fit the present results. A non-negligible contribution of the continuum cross section was found for the ^{6}Li(e,π^+) result in a previous paper [17].

The photon energy dependence of the resonance cross sections in the (γ,π^+), although expected to be small, is not known. Therefore, the contribution of the continuum cross section in the (γ,π^+) reaction is uncertain. In the present study, the continuum part $C(T_\pi)$ in Eq. (5) will be neglected. Even though the information for the continuum cross section is uncertain, the integrated cross sections of the resonances are clearly determined because the present analysis is performed by fitting to the reference spectrum at around only about 5 MeV from the endpoint energy for each resonance.

The results of differential photopion cross sections are shown in Table II. In the energy region below 8.5 MeV in

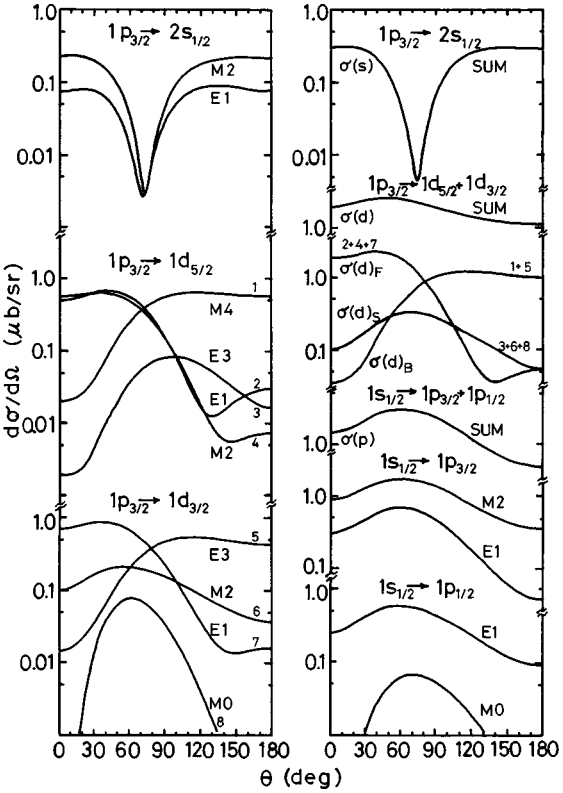

FIG. 4. Angular distribution curves for the (γ,π^+) reaction on ^{7}Li and ^{9}Be calculated using DWIA and the single particle shell model wave function. Components for the possible multipolarity due to the transitions from the $1p_{3/2}$ shell to the $2s_{1/2}$, $1d_{5/2}$ or $1d_{3/2}$ shell and those from the $1s_{1/2}$ shell to the $1p_{3/2}$ or $1p_{1/2}$ shell are shown. Also shown are the sum for the transition groups: $\sigma(s)$, $1p_{3/2}\rightarrow 2s_{1/2}$; $\sigma(d)$, $1p_{3/2}\rightarrow 1d_{5/2}+1d_{3/2}$; $\sigma(p)$, $1s_{1/2}\rightarrow 1p_{3/2}+1p_{1/2}$ and the component sum for three typical separated patterns in $\sigma(d)$:$\sigma(d)_F$, forward group; $\sigma(d)_s$, symmetric group; $\sigma(d)_B$, backward group.

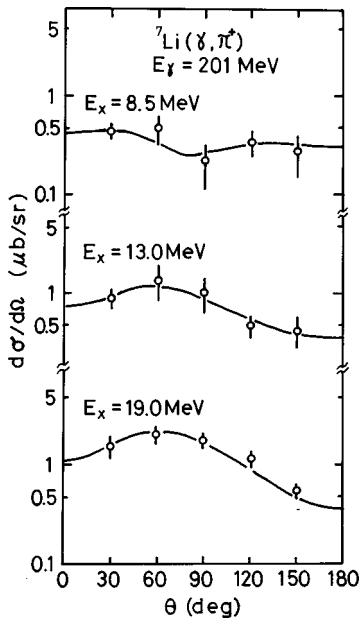

FIG. 5. Angular distributions of photoproduced π^+ from ^{7}Li. Comparison is performed using the DWIA calculation results shown in Fig. 4 by multiplying probable factors given in Table III.

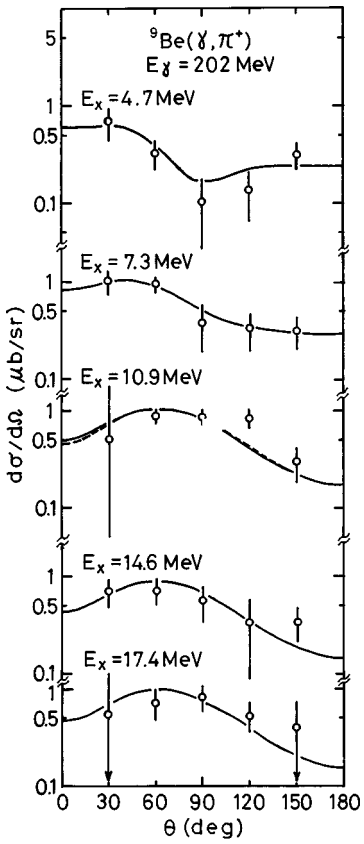

FIG. 6. Angular distributions of photoproduced π^+ from ^{9}Be. Comparison is performed using the DWIA calculation results (see caption for Fig. 5). For $E_x = 10.9$ MeV, the solid curve and the broken curve show $0.35\sigma(p)$ and $\sigma(d)_s + 0.24\sigma(p)$, respectively.

^{7}Li and below 4.7 MeV in ^{9}Be, the quoted cross sections are the average values over all angles, because the small counting rates at each individual angle does not allow the extraction of a statistically significant differential cross section. Determination of the widths is impossible because the statistical error of the present data is not adequate for such analysis, as mentioned previously.

III. DISCUSSION OF RESULTS

Angular distributions of photoproduced π^+ were calculated using the DWIA code written by Ohtsubo [14]. For the *T*-matrix element in the DWIA calculation, the elementary amplitude $\vec{J}_5$ given by the expression of Chew-Goldberger-Low-Nambu (CGLN) [15] was used. The distorted wave of emitted pions was obtained by solving the Klein-Gordon equation, with the energy-dependent optical potential parameter set E given by Carr, McManus, and Stricar-Bauer [16].

For the charge exchange nucleon transition in ^{7}Li and ^{9}Be, single particle wave functions were used for both the initial states in the $1p_{3/2}$ and $1s_{1/2}$ shells, and the final states in the $1p_{3/2}$, $1p_{1/2}$ and s-d shells. The results of the calculations for the angular distribution are approximately equal in both nuclei, as shown in Fig. 4, in which all of the allowed multipolarities for each nucleon transition are shown. Also shown are the sum distributions for each the components: $\sigma(s)$, $1p_{3/2} \rightarrow 2s_{1/2}$; $\sigma(d)$, $1p_{3/2} \rightarrow 1d_{5/2} + 1d_{3/2}$; $\sigma(p)$, $1s_{1/2} \rightarrow 1p_{3/2} + 1p_{1/2}$, and the classified partial sum distribution in a group having three typical angular distribution patterns for all of the components of $\sigma(d)$: $\sigma(d)_F$, forward group; $\sigma(d)_s$, symmetric group; $\sigma(d)_B$, backward group, as shown in Fig. 4.

The experimental angular distributions $(d\sigma_{(\gamma,\pi)}/d\Omega)_i$ for the strong groups of photoproduced π^+ are plotted in Figs. 5 and 6 (hereafter, $d\sigma/d\Omega$ denotes $(d\sigma_{(\gamma,\pi)}/d\Omega)_i$ and E_x denotes E_{x_i}) and compared to the DWIA calculations. Since the residual states at E_x observed in the present experiment are probably a complex of states within the energy resolution, some ambiguity is encountered in comparing the experimental results and DWIA calculations. In order to obtain reasonable fit to the experimental results, the distributions shown in Fig. 4 were selected and summed using the scaling factors to reproduce the experimental pattern. The most probable scaling factors are listed in Table III, and the results are shown in Figs. 5 and 6. For the group at $E_x = 0$ in ^{9}Be(γ,π^+), the large scaling factor in Table III is obtained from a previous study [5], which suggested that the magnitude of the factor may be due to the improper nuclear wave

TABLE III. Scaling factors to be multiplied by the DWIA single particle shell model calculations to fit the experimental angular distributions.

		Coefficients					
	E_x (MeV)	$\sigma(s)$[a]	$\sigma(d)$[b]	[$\sigma(d)_F$[c]	$\sigma(d)_S$[d]	$\sigma(d)_B$[e]]	$\sigma(p)$[f]
^{7}Li	0		($\geqslant 1$ of $1p_{3/2} \rightarrow 1p_{3/2}$ transition)				
	~6		~0.16				
	8.5	0.60	0.12				
	13.0		0.23				0.20
	19.0						0.75
	Sum	0.60	~0.51				0.95
^{9}Be	0		($\geqslant 1$ of $1p_{3/2} \rightarrow 1p_{3/2}$ transition)[g]				
	4.7	0.80		0.20			
	7.3			0.45		0.27	
	10.9[h]				0		0.35
					1		0.24
	14.6						0.30
	17.4						0.32
	Sum[h]	0.80		0.65	0	0.27	0.97
		0.80		0.65	1	0.27	0.86

[a]Cross section summed over all transitions on $(1p_{3/2} \rightarrow 2s_{1/2})_{(E1+M2)}$.

[b]Cross section summed over all transitions on $(1p_{3/2} \rightarrow 1d_{5/2})_{(E1+M2+E3+M4)} + (1p_{3/2} \rightarrow 1d_{3/2})_{(M0+E1+M2+E3)}$.

[c]Cross section sum of the components having a forward pattern in an angular distribution given by $(1p_{3/2} \rightarrow 1d_{5/2})_{(E1+M2)} + (1p_{3/2} \rightarrow 1d_{3/2})_{(E1)}$.

[d]Cross section sum of the components having an approximately symmetric pattern in an angular distribution given by $(1p_{3/2} \rightarrow 1d_{5/2})_{(E3)} + (1p_{3/2} \rightarrow 1d_{3/2})_{(M0+M2)}$.

[e]Cross section sum of the components having a backward pattern in an angular distribution given by $(1p_{3/2} \rightarrow 1d_{5/2})_{(M4)} + (1p_{3/2} \rightarrow 1d_{3/2})_{(E3)}$.

[f]Cross section summed over all transitions on $(1s_{1/2} \rightarrow 1p_{3/2})_{(E1+M2)} + (1s_{1/2} \rightarrow 1p_{1/2})_{(M0+E1)}$.

[g]See Ref. [5].

[h]Two similar sets of coefficients are possible for the same result.

TABLE IV. The excitation energy E_x of the major spin-isospin flip giant resonance states examined using the single nucleon transitions in (γ,π^+) reaction on $1p_{3/2}$ shell nuclei. Spin and parity, J^π, are given in parenthesis when determined.

Target nucleus	^{6}Li(1^+)	^{7}Li($3/2^-$)	^{9}Be($3/2^-$)	^{11}B($3/2^-$)	^{12}C(0^+)	^{13}C($1/2^-$)
Lowest energy of $T_>$ state (MeV)	3.56	11.24	14.39	12.56	15.11	15.11
Residual nucleus	^{6}He	^{7}He	^{9}Li	^{11}Be	^{12}B	^{13}B
Transition	E_x (MeV)					
$1p_{3/2}\rightarrow 1p_{3/2}+1p_{1/2}$	$0(0^+)$[a] $1.8(2^+)$[a]	$0(3/2^-)$[b]	$0(3/2^-)$[c]		$0(1^+)$[d] $0.95(2^+)$[d]	$0(3/2^-)$[e]
$1p_{3/2}\rightarrow s$-d	7[f]	~ 6[b]	4.7[b]	$0(1/2^+)$[g] 2.7[g]	4.5[i] $\begin{bmatrix}2^-\\4^-\end{bmatrix}$	3.5[h] 6.4[h]
	9[f]			5.2[g] 6.8[g] 9.4[g]	$\begin{bmatrix}7.0^{j}\begin{bmatrix}2^-\\1^-\end{bmatrix}\\7.5^{k}\end{bmatrix}$	$\begin{bmatrix}9.0^{h}\\9.5^{k}\end{bmatrix}$
	12[f]	8.5[b]	7.3[b]	12.0[g] 16.4[g] 17.5[g]	10[k] 13[l]	13[k]
	13.6[j]	13.0[m]	10.9[n]			
$1s_{1/2}\rightarrow 1p_{3/2}+1p_{1/2}$	17.7[j] 24.0[j]	13.0[m] 19.0[b]	10.9[n] 14.6[b] 17.4[b]			

[a]See Ref. [4].
[b]Present results; see Table III.
[c]See Ref. [5].
[d]See Refs. [6,8].
[e]See Refs. [8,9].
[f]Transition modes have not yet been studied thoroughly; however, the present mode is assumed based on strength consideration. See Ref. [17].
[g]See Ref. [18].
[h]See Refs. [8,10].
[i]See Refs. [7,8].
[j]See Ref. [17].
[k]See Ref. [8].
[l]Present transition mode is assumed by angular distribution. See Ref. [8].
[m]Present result, see Table III, $0.23(1p_{3/2}\rightarrow 1d_{5/2}+1d_{3/2})+0.20(1s_{1/2}\rightarrow 1p_{3/2}+1p_{1/2})$.
[n]Present result, see Table III, $0.35(1s_{1/2}\rightarrow 1p_{3/2}+1p_{1/2})$, or $(1p_{3/2}\rightarrow 1d_{5/2})_{(E3)}+(1p_{3/2}\rightarrow 1d_{3/2})_{(M0+M2)}$ $+0.24(1s_{1/2}\rightarrow 1p_{3/2}+1p_{1/2})$.

function for the residual ground state. In ^{7}Li(γ,π^+), a similar conclusion can be obtained for the group at $E_x=0$, and the group at $E_x\approx 6$ MeV is compared to $\sigma(d)$, which corresponds to the low excited states.

As seen in Table III, the total of the experimental (γ,π^+) cross section at E_x is approximately equal to half of the sum of the DWIA result for the single nucleon transitions. Note that part of strength, which is fragmented over the entire energy region of the experiment, does not appear as observable peaks in the experiment. If these missing strengths were added, the complete π^+ yields would be closer to the theoretical estimates. Therefore, the total experimental cross section of the (γ,π^+) groups are expected to satisfy the sum rule for the spin-isospin flip giant resonance.

The result of the angular distribution agrees with the fact that the single particle transitions from the $1p_{3/2}$ shell lead mainly to the lower and middle energy groups of the residual states, whereas those from the $1s_{1/2}$ shell in the nuclear core lead predominantly to the higher energy group of the residual states. This conclusion is consistent with the systematics for energy of the single particle shell models as discussed below.

Major spin-isospin flip giant resonance states observed in the (γ,π^+) reaction on $1p_{3/2}$ shell nuclei and the corresponding single nucleon transitions are summarized, together with results of previous studies, in Table IV. The states at 7, 9, and 12 MeV in ^{6}He have not been reported for other reactions [19] and the transition modes have not been thoroughly in previous studies; however, these states might be

TABLE V. Separation energies, $E_i(1s)$ and $E_i(1p)$, and widths for the $1s_{1/2}$ and $1p_{3/2}$ shell nucleons obtained from the $(e,e'p)$ and $(p,2p)$ experiments. The Q value of these reactions and the estimates of the difference energies $\Delta E_{s-p}=E_i(1s)-E_i(1p)$ are shown. Energy is given in MeV.

Nucleus	^{6}Li	^{7}Li	^{9}Be	^{11}B	^{12}C
Q (MeV)	-4.59	-9.98	-16.89	-11.23	-15.96
$(e,e'p)$	Ref. [24]	Ref. [24]	Ref. [24]		Ref. [25]
$E_i(1s)$	22.6 ± 0.2	26.0 ± 0.2	27.1 ± 0.4 37.5 ± 0.4		36.9 ± 0.3
Width[a]	18.4 ± 0.6	20.3 ± 0.6	8.7 ± 0.6 15.3 ± 1.0		19.8 ± 0.5
$E_i(1p)$	4.5 ± 0.2	10.1 ± 0.2	18.1 ± 0.2		15.5 ± 0.1
Width	8.2 ± 0.3	7.7 ± 0.3	9.8 ± 0.5		6.9 ± 0.1
ΔE_{s-p}	18.1 ± 0.3	15.9 ± 0.3	14.2[b]		21.4 ± 0.3
Width	20.1	21.7	~22[b]		21.0
			Ref. [26]		Ref. [27]
$E_i(1s)$			32 ± 1		38.1 ± 1.0
Width			9[c]		~20
$E_i(1p)$			18.0 ± 0.3		7.5 ± 0.4
Width			small[c]		small[c]
ΔE_{s-p}			14 ± 1		20.6 ± 1
Width			9		~20
Mean value					
ΔE_{s-p}	18.1 ± 0.3	15.9 ± 0.3	14		21.3 ± 0.3[d]
Width	20.1	21.7			~21
$(p,2p)$	Ref. [28]	Ref. [28]	Ref. [28]	Ref. [28]	Ref. [29]
$E_i(1s)$	22.7 ± 0.3	25.5 ± 0.4	25.4 ± 0.5		35.5 ± 1.0
Width	4.0	5.9	6.3	10.9 ± 0.4	13
$E_i(1p)$	4.9 ± 0.3	11.8 ± 0.3	16.4 ± 0.3	14.6 ± 0.5	15 ± 0.5
Width	3.3	5.3	4.0	21.2 ± 0.5	4
ΔE_{s-p}	17.8 ± 0.4	13.7 ± 0.5	9.0 ± 0.6		20.5 ± 1.1
Width	5.2	7.9	7.4		15
	Ref. [30]	Ref. [30]	Ref. [30]		
ΔE_{s-p}	16.7	13.4 ± 0.5 15.3 ± 0.3	9 16		
Width			6 8		
Mean value					
ΔE_{s-p}	17.3	13.6 ± 0.4[e]	9		20.5 ± 1.1
Width	(5.2)	(7.9)	7		15

[a]All widths are shown in FWHM.
[b]Sum of the two $1s$ groups.
[c]Width estimated from data in reference.
[d]Weighted mean.
[e]Lowest difference energy.

seen in the spectra of the (π^-,γ) [20,21], (n,p) [22] or (γ,π^+) reactions [17]. For these states, $1p_{3/2}\rightarrow s$-d was assumed based on transition strength. The resonance states at 7.0 and 7.5 MeV in ^{12}B are the (e,π^+) result and the tagged photon result, respectively. The result of 7.0 MeV may be the same resonance at 7.5 MeV, because the error of fitting of the reference curve to the (e,π^+) spectra may be about 0.5 MeV, as shown in Fig. 3. The same situation also applies to the 9.0 and 9.5 MeV states in ^{13}B.

The energies of the residual states for the giant resonances, E_R, are given by

$$E_R=E_i+E_f+\Delta E, \tag{9}$$

where E_i is the separation energy of the initial shell state, E_f is the binding energy of the final shell state and ΔE is the correction energy for particle-hole interaction, etc. in giant resonance [23].

The separation energies E_i of a nucleon in the shell model orbits have been examined experimentally using $(p,2p)$, $(e,e'p)$, and other reactions. The results of E_i for $1s_{1/2}$ and $1p_{3/2}$ shell nucleons obtained by the $(e,e'p)$ and $(p,2p)$ experiments are listed in Table V. Also shown in the table is the residual energy after the transition of a nucleon from the $1s_{1/2}$ shell to the $1p_{3/2}$ shell, which is given approximately by the difference energy $\Delta E_{s-p}=E_i(1s)-E_i(1p)$. The mean values of ΔE_{s-p} and the widths of each energy are

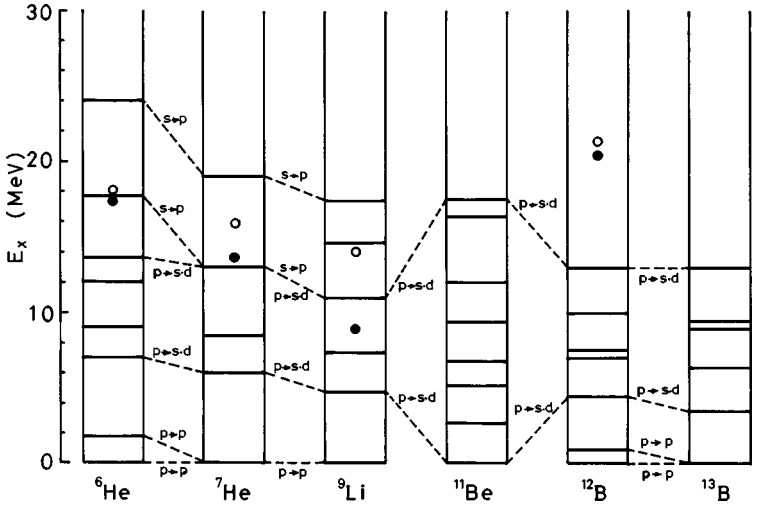

FIG. 7. Energy scheme of the spin-isospin flip giant resonances in $1p_{3/2}$ shell nuclei. Thick horizontal lines show the residual states or resonances in (γ,π^+) reactions, as shown in Table IV. The result at 7.0 MeV in ^{12}B and 9.0 MeV in ^{13}B may be the same resonance at 7.5 and 9.5 MeV, respectively, considering the error in the present fitting method. The region contributed by the same main transition of nucleon in the single particle shell model is shown by a broken line between nuclei indicated by the main transition. Open circles and closed circles are the mean energy of $1s_{1/2}$ hole states determined by $(e,e'p)$ and $(p,2p)$ data, respectively, as given in Table V.

given when possible. The widths of the separation energy are very large, as shown in the table; therefore, ΔE_{s-p} gives the mean energy of the $1s_{1/2}$ hole residual states.

The energy scheme of the spin-isospin flip giant resonances in $1p_{3/2}$ shell nuclei are summarized in Fig. 7 for the systematic study. Thick horizontal lines show the residual states in the (γ,π^+) reaction given in Table IV. The region contributed by the main transition of the nucleon in the single particle shell model is connected between nucleus by broken lines indicated by $p\rightarrow p$ for the $1p_{3/2}\rightarrow 1p_{3/2}+1p_{1/2}$ transition, $p\rightarrow s\cdot d$ for the $1p_{3/2}\rightarrow s-d$ transition and $s\rightarrow p$ for the $1s_{1/2}\rightarrow 1p_{3/2}+1p_{1/2}$ transition. Open circles and closed circles show the mean energy of $1s_{1/2}$ hole states ΔE_{s-p} determined by the $(e,e'p)$ and $(p,2p)$ reactions, respectively, as given in Table V.

As shown in Fig. 7, the lowest states, except for the case of ^{11}Be, are described well by the main transition within the $1p$ shell. In the case of ^{11}Be, J^π of the ground state is $1/2^+$, and this state is attributed to the main transition of $1p_{3/2}\rightarrow 2s_{1/2}$. The $1p_{3/2}\rightarrow s-d$ transition contributes to the middle energy region of the spin-isospin flip giant resonances in ^{6}He, ^{7}He, and ^{9}Li, and to almost all of the resonances in ^{11}Be, and ^{12}B and ^{13}B except the lowest energy region. The transition of the core nucleon $1s_{1/2}\rightarrow 1p_{3/2}+1p_{1/2}$ appears in the high energy region only in ^{6}He, ^{7}He, and ^{9}Li. These highly excited states are included in the broad energy region around the $1s_{1/2}$ hole state shown by the circles for mean energy. The core transition mode is not seen for ^{11}Be, ^{12}B, and ^{13}B. This is because the $1s_{1/2}$ hole energy is too high to be observed, as shown by the data of ^{12}B, and also because the $1p$ shell, which is the final state for one harmonic transition from the core, are mostly blocked.

The data obtained by reactions similar to (γ,π^+) are listed in Table VI. The table shows the states or groups clarified by the (π^-,γ) experiments on ^{6}Li [20,21,31], ^{7}Li, ^{9}Be, ^{11}B [21,31], ^{12}C [20,31,32], and ^{13}C [33], and from the (n,p) experiments on ^{6}Li, ^{7}Li [22], and ^{12}C [34]. In addition, the resonance widths are shown when estimation is possible. Table VI also shows the theoretical results of the energy for the residual states as calculated by the shell model. The theoretical cross sections for the strong transition of (γ,π^+) are given at $\theta=90°$ on ^{6}Li [35], ^{12}C, ^{13}C [14,36] and for that of (π^-,γ) on ^{7}Li, ^{9}Be, ^{11}B [37]. In Table VI, the states are shown by the main transitions of p shell$\rightarrow p$ shell, p shell $\rightarrow s-d$ shell and s shell$\rightarrow p$ shell. The distribution of states are reasonable in these reactions.

The (π^-,γ) reaction by stopped π^- is the inverse reaction of the (γ,π^+) reaction, as mentioned previously. The interaction is similar, except for the photon and pion energy. The momentum transfer is fixed in the (π^-,γ) reaction, in contrast that in the (γ,π^+) reaction, in which momentum transfer is variable. The π^- in the (π^-,γ) reaction is captured from the $1s$ or $2p$ state of atomic orbit, but the π^+ in the (γ,π^+) reaction is emitted along with some energy due to interaction with nucleons inside the nucleus, which is described by the optical potential. Therefore, ϕ_π^* is quite different in both reactions. The photon energy is less than the threshold energy in the (π^-,γ) reaction and near 200 MeV in the present (γ,π^+) reaction. These differences influence the components of the elementary operator F_n, which is given by similar expressions in both reactions.

The photon spectra measured by the (π^-,γ) experiments directly indicate the resonance structure; however, the π^+ spectra obtained in the (γ,π^+) experiments through electron bombardment are folded by the continuous photon spectra, which show the indirect resonance structure.

Comparison of the results of the (π^-,γ) experiments and the present (γ,π^+) results at $\theta=30°$ reveals that the momentum transfers of these two reactions are nearly equal. The photon spectra of (π^-,γ) on Li and ^{9}Be [21,23] large continuums are estimated and fitted to the results; however, the present (γ,π^+) results on these nuclei do not indicate any large contributions of the continuum.

The continuum cross sections and background are estimated by tagged (γ,π^+) experiments on ^{12}C and ^{13}C. The continuum cross sections are not large in comparison with

TABLE VI. Comparison of the energy E_x (in MeV) of the residual states and/or groups in giant resonances examined in the (γ,π^+), (π^-,γ), and (n,p) reaction experiments and by the theoretical calculations using the shell model on (γ,π^+) and (π^-,γ) reactions. When states in more than three groups are distributed, the energy region of the groups is shown. Nonexistent states are indicated by a hyphen. When the transition mode is not estimated, the energy is shown in parenthesis and is included in the probable transition group.

Target nucleus	^{6}Li	^{7}Li	^{9}Be	^{11}B	^{12}C	^{13}C
Residual nucleus	^{6}He	^{7}He	^{9}Li	^{11}Be	^{12}B	^{13}B
			p shell→p shell transition			
Experiment						
(γ,π^+)[a]	0, 1.8	0	0	–	0–0.95	0
(π^-,γ)	0, 1.8[b]	0[b]	0, 2.6[b]	0[b]	0–2.6[b]	0[c]
(n,p)	0, 1.8[d]	0[d]			0, 0.95[e]	
Theory						
(γ,π^+)	0, 1.8[f]				0[g,h]	0[h]
(π^-,γ)	0–7[i]	0[i]	0[i]	–[i]		0[i]
			p shell→s-d shell transition			
Experiment						
(γ,π^+)[a]	7–13.6	~6–13	4.7–10.9	0–17.5	4.5–13	3.5–13
(π^-,γ)	5, 14.5[j]	8, 12[j]	4.2, 7[j]	(0–12)[j]	4.2–8[j]	3.5–10[c]
Width	2.5, 6	5.5, 1.5	~0, 8	~0–16	1.5,1.5	0–4
(n,p)	(7, 15.5)[d]	6[d]			4.4–9.5[e]	
Width	4, 6	6				
Theory						
(γ,π^+)	9–15.5[f]				1–9[g]	3–12[g]
(π^-,γ)	9–14[i]	1–13[i]	4–11, 15–24[i]	0–12[i]		3–20[i]
			s shell→p shell transition			
Experiment						
(γ,π^+)[a]	17.7, 24	13–19	10.9–17.4	–	–	–
(π^-,γ)	22.5[j]	19[j]	17.5[j]	–[j]	–[j]	–[c]
Width	6	6	12			
(n,p)	25[d]	20[d]			–[e]	
Width	8	9				
Theory						
(γ,π^+)	13–29[f]				–[g]	–[g]
(π^-,γ)	14–30[i]	15.5–20.5[i]	13.7[i]	–[i]		–[i]

[a]References are shown in Table IV.
[b]See Ref. [31].
[c]See Ref. [33].
[d]See Ref. [22].
[e]See Ref. [34].
[f]See Ref. [35].
[g]See Ref. [36].
[h]See Ref. [14].
[i]See Ref. [37].
[j]See Ref. [21].

resonance structure [8]. Previous studies have revealed that the π^+ total yields produced from the (e,π^+) reaction are approximately an order smaller than theoretical estimates found using the Fermi gas model [38–40]. Since the cross section of the resonance peaks are as large as the spin-isospin flip giant resonance estimates, a reduction of the continuum in the (γ,π^+) reaction appears to occur. The difference between the continuums of the (γ,π^+) and (π^-,γ) reactions may depend on the different energies of the corresponding photon and pion.

The resonance energies in the present results on ^{7}Li and ^{9}Be at $\theta=30°$ are compared to the photon spectra of the (π^-,γ) reaction having nearly the same momentum transfer, and a similar nuclear response is expected. Statistical uncertainty appears to make finding the resonance structure after subtraction of the large continuum in the highly excited energy region of the (π^-,γ) results difficult. Under the uncertainty of the results for both reactions, the resonances of the ^{7}Li(γ,π^+) reaction at $E_x=8.5$, 13, and 10 MeV (relative strengths are 0.4, 0.9, and 1.5, respectively) appear to correspond to the photon spectra from the ^{7}Li(π^-,γ) result [21,31], except at $E_x=13$ MeV, where two separate resonances appear to exist around 13 MeV. The resonances of the ^{9}Be(γ,π^+) reaction at $E_x=4.7$, 7.3, 10.9, 14.6, and 17.4 MeV (relative strengths are 0.7, 1.0, 0.5, 0.7, and 0.6, respectively) do not contradict the ^{9}Be(π^-,γ) result [21,31] if the result is smeared after the subtraction of large continuums. Although the experimental and theoretical results are not always in agreement, similarity of the distribution of the resonances can be expected.

The results of the (n,p) reactions may be similar to the photonuclear reactions in the giant resonance energy region. The DWBA analysis of the (n,p) reactions on ^{6}Li and ^{7}Li in Ref. [22] shows that the strong broad resonances are spin nonflip giant dipole resonances. The analysis of the $^{12}C(n,p)$ reaction indicates that both spin flip and nonflip transitions contribute to the energy region [34]. The measured resonance spectra appear to be equivalent for the (n,p) and (π^-,γ) experiments on ^{6}Li and ^{7}Li. Since the (π^-,γ) reaction typically depends on spin flip transition, the resonance mode for (n,p) and that obtained from the (π^-,γ) and (γ,π^+) results are different. This may be a result of the considerable difference in interacting energies. Thus, the results show reasonable agreement among the various reactions examined.

The systematics for spin-isospin flip mode giant resonances was examined in the present study by comparative analysis of (γ,π^+) data with other charge exchange reactions, as shown in Table VI. The DWIA analysis using the single particle shell model gives reasonable results for the (γ,π^+) reaction on the $1p_{3/2}$ shell nuclei. Extraction of spin-isospin flip giant resonance and analysis of their configurations appears to be a promising application of the (γ,π^+) experiment. Since the main source of ambiguity in the analysis of the π^+ electroproduction experiments arises from the fitting procedure for continuous photon spectra, improved statistics experiments using tagged photons should give more precise information for the spin-isospin flip giant resonance.

The light nuclei discussed for shell dependence in the present paper are described by cluster model as well. The cluster model of ^{7}Li was examined thoroughly together with ^{6}Li by photodisintegration and other reactions. The clusters for ^{9}Be were not discussed in detail due to the complexity involved, but a recent qualitative study on photodisintegration has clarified the cluster nature [2]. The interplay of both models elucidated by photonuclear giant resonance and by photopion production should provide important information in the study of nuclear structure.

An important extension of the present experimental method and analysis is suggested for application to study for the states of the hypernuclei by selectively detecting K^+ produced from nuclei by electron or bremsstrahlung bombardment.

ACKNOWLEDGMENTS

The authors would like to thank the photopion group and machine crew of the Laboratory of Nuclear Science, and the late Professor T. Yamaya, Department of Physics, Tohoku University, for their help during the experiment. The authors are also very grateful to Professor K. Min, Department of Physics, Rensselaer Polytechnic Institute, for his careful proofreading of the manuscript.

[1] K. Langanke, in *Advances in Nuclear Physics, Vol. 21*, edited by J. W. Negele and E. Vogt (Plenum, New York, London, 1994), p. 85.
[2] K. Shoda and T. Tanaka, Phys. Rev. C **59**, 239 (1999).
[3] A. Nagl, V. Devanathan, and H. Überall, *Nuclear Pion Photoproduction* (Springer-Verlag, Berlin, Heidelberg, 1991); B. C. Doyle, Nimai C. Mukhopadhyay, and R. S. Wittman, Phys. Rev. C **52**, 1957 (1995).
[4] K. Shoda, O. Sasaki, and T. Kohmura, Phys. Lett. **101B**, 124 (1981).
[5] P. K. Teng, A. Chaudhury, J. J. LeRose, K. Min, D. Rowley, B. O. Sapp, P. Stoler, E. J. Winhold, P. F. Yergin, A. M. Bernstein, K. I. Blomqvist, G. Franklin, N. Paras, M. Pauli, and B. Schoch, Phys. Rev. C **26**, 1313 (1982); K. Shoda, M. Yamazaki, M. Torikoshi, O. Sasaki, H. Tsubota, and B. N. Sung, Nucl. Phys. **A403**, 469 (1983).
[6] K. Shoda, H. Ohasi, and K. Nakahara, Nucl. Phys. **A350**, 377 (1980).
[7] K. Min, E. J. Winhold, K. Shoda, H. Tsubota, H. Ohasi, and M. Yamazaki, Phys. Rev. Lett. **44**, 1384 (1980).
[8] H. Choi, T. Kobayashi, K. Min, L. Y. Murphy, P. F. Yergin, J. Shaw, D. M. Skopik, J. M. Vogt, H. T. Chung, J. C. Kim, H. Tsubota, and K. Shoda, Nucl. Phys. **A579**, 539 (1994).
[9] K. Shoda, M. Yamazaki, M. Torikoshi, H. Tsubota, K. Min, E. J. Winhold, and A. M. Bernstein, Phys. Rev. C **27**, 443 (1983).
[10] K. Min, E. J. Winhold, K. Shoda, M. Torikoshi, M. Yamazaki, O. Sasaki, H. Tsubota, and B. N. Sung, Phys. Rev. C **28**, 464 (1983).
[11] T. Kobayashi, K. Takeshita, A. Kagaya, H. Tsubota, and K. Shoda, J. Phys. Soc. Jpn. **58**, 1570 (1989).
[12] L. I. Schiff, Phys. Rev. **83**, 252 (1951).
[13] L. Tiator and L. E. Wright, Nucl. Phys. **A379**, 407 (1982).
[14] H. Ohtsubo (private communication); T. Sato, K. Koshigiri, and H. Ohtsubo, Z. Phys. A **320**, 507 (1985).
[15] G. F. Chew, M. L. Goldberger, F. E. Low, and Y. Nambu, Phys. Rev. **106**, 1345 (1957).
[16] J. A. Carr, H. McManus, and K. Stricker-Bauer, Phys. Rev. C **25**, 952 (1982).
[17] K. Shoda, M. Torikoshi, O. Sasaki, S. Tôyama, T. Kobayashi, A. Kagaya, and H. Tsubota, Phys. Rev. C **33**, 2179 (1986).
[18] T. Yamaya, M. Saitoh, H. Yamazaki, T. Taniuchi, K. Shoda, and H. Tsubota, Phys. Rev. C **51**, 493 (1995).
[19] F. Ajzenberg-Selove, Nucl. Phys. **A490**, 1 (1988).
[20] H. W. Baer, K. M. Crowe, and P. Truöl, *Advances in Nuclear Physics* (Plenum, New York, London, 1977), Vol. 9, p. 177.
[21] E_x are estimated from E_γ in (π^-,γ) results by J. P. Perroud, in *Photopion Nuclear Physics*, edited by P. Stoler (Plenum, New York, London, 1979), p. 69.
[22] F. Brady, G. A. Needham, J. L. Romero, C. M. Castaneda, T. D. Ford, J. L. Ullmann, and M. L. Webb, Phys. Rev. Lett. **51**, 1320 (1983).
[23] G. E. Brown and M. Bolsterli, Phys. Rev. Lett. **3**, 472 (1959).
[24] K. Nakamura, S. Hiramatsu, T. Kamae, H. Muramatsu, N. Izutsu, and Y. Watase, Nucl. Phys. **A296**, 431 (1978).
[25] K. Nakamura, S. Hiramatsu, T. Kamae, H. Muramatsu, N. Izutsu, and Y. Watase, Nucl. Phys. **A268**, 381 (1976).
[26] J. Mougey, Nucl. Phys. **A335**, 35 (1980).
[27] J. Mougey, M. Bernheim, A. Bussière, A. Gillebert, P. X. Ho, M. Priou, D. Royer, I. Sick, and G. J. Wagner, Nucl. Phys. **A262**, 461 (1976).

[28] H. Tyren, S. Kullander, O. Sundberg, R. Ramachandran, P. Isacsson, and T. Berggren, Nucl. Phys. **79**, 321 (1966).

[29] G. Landaud, J. Yonnet, S. Kullander, F. Lemeilleur, P. U. Renberg, B. Fagerström, A. Johansson, and G. Tibell, Nucl. Phys. **A173**, 337 (1971).

[30] J. C. Roynette, M. Arditi, J. C. Jacmart, F. Mazloum, M. Riou, and C. Ruhla, Nucl. Phys. **A95**, 545 (1967).

[31] J. P. Perroud, A. Perrenoud, J. C. Alder, B. Gabioud, C. Joseph, J. F. Loude, N. Morel, M. T. Tran, E. Winkelmann, H. Von Fellenberg, G. Strassner, P. Truöl, W. Dahme, H. Panke, and D. Renker, Nucl. Phys. **A453**, 542 (1986).

[32] J. C. Alder, W. Dahme, B. Gabioud, C. Joseph, J. F. Loude, N. Morel, H. Panke, A. Perrenoud, J. P. Perroud, D. Renker, G. Strassner, M. T. Tran, P. Truöl, and E. Winkelman, in *Photopion Nuclear Physics*, edited by P. Stoler (Plenum, New York, London, 1979), p. 101.

[33] C. J. Martoff, J. A. Bistirlich, C. W. Clawson, K. M. Crowe, M. Koike, J. P. Miller, S. S. Rosenblum, W. A. Zajc, H. W. Baer, A. H. Wapstra, G. Strassner, and P. Truöl, Phys. Rev. C **27**, 1621 (1983).

[34] F. P. Brady, T. D. Ford, G. A. Needham, J. L. Romero, D. S. Sorenson, C. M. Castaneda, J. L. Drummond, E. L. Hjort, B. McEachern, and N. S. P. King, Phys. Rev. C **43**, 2284 (1991).

[35] R. A. Eramzhyan, T. D. Kaipov, and S. S. Kamalov, Z. Phys. A **322**, 321 (1985).

[36] R. A. Eramzhyan, M. Gmitro, S. S. Kamalov, T. D. Kaipov, H. Kissener, and O. Richter, Czech. J. Phys. **41**, 1113 (1991).

[37] H. R. Kissener, G. E. Dogotar, R. A. Eramzhyan, and R. A. Sakaev, Nucl. Phys. **A312**, 394 (1978).

[38] K. Shoda, S. Toyama, M. Torikoshi, O. Sasaki, and T. Kobayashi, Nucl. Phys. **A486**, 512 (1988).

[39] K. Shoda, T. Kobayashi, O. Sasaki, and S. Toyama, Nucl. Phys. **A486**, 526 (1988).

[40] K. Shoda, O. Sasaki, K. Takeshita, T. Taniuchi, and H. Tsubota, J. Phys. Soc. Jpn. **63**, 478 (1994).